



A WAVE APPROACH TO ESTIMATING FREQUENCY-DEPENDENT DAMPING UNDER TRANSIENT LOADING

J. G. MCDANIEL AND P. DUPONT

Aerospace & Mechanical Engineering, Boston University, Boston, MA 02215, U.S.A.

AND

L. SALVINO

Naval Surface Warfare Center, Carderock Division, West Bethesda, MD 20817, U.S.A.

(Received 29 December 1998 and in final form 11 October 1999)

A wave model is proposed for estimating damping loss factor as a function of frequency for a beam with arbitrary transient loading applied through the boundary conditions. In contrast to modal methods which provide measures of damping only at the modal frequencies of the test structure, the damping factor is determined over discrete, but regularly spaced, frequency values associated with the temporal sampling frequency. This makes it possible to predict or simulate damping in complex structures built from the tested component. Numerical and experimental data from a free-free beam are used to validate the approach.

© 2000 Academic Press

1. INTRODUCTION

A new method is presented for estimating the frequency-dependent loss factor of a damped vibrating beam from its transient response measured at several locations. The method, which is applied here to numerical and experimental beam data, uses the Fourier transform of the measured transient responses. Knowledge of the beam's equation of motion is used to express the transformed responses at any frequency as a sum of four damped waves. The loss factor is a simple function of the spatial decays of these waves and may be estimated at any frequency for which the Fourier transform can be accurately obtained. For short-time excitations, this method allows one to estimate the loss factor at many frequencies, thus overcoming the inherent limitations of modal descriptions that only estimate the loss factor at the natural frequencies of the structure.

In recent years, a number of authors have developed representations of structural response in terms of damped waves described by complex wavenumbers. For example, Plona *et al.* [1] presented theoretical and experimental studies of the complex wavenumbers of axisymmetric waves propagating in cylindrical shells in contact with various acoustic media. Their experimental results were generated by

exciting the shell with one cycle sinewave bursts centered at the frequency of interest. Vollman *et al.* [2] studied the complex wavenumbers of up to 40 waves propagating in a cylindrical shell in contact with a viscoelastic medium. Their work, which also presented theoretical and experimental results, used a complex spectrum estimation technique. McDaniel *et al.* [3] demonstrated that the complex wavenumbers, amplitudes, and loss factor of mechanically excited damped beam could be determined from a small array of accelerometers at any frequency of excitation. Their approach used an iterative scheme that minimized the error between the wave description and the measured responses by adjusting the complex wavenumbers and amplitudes.

The problem addressed here is significantly different than those mentioned above in that the excitation occurs over a very short time period. Consequently, the structure is in free vibration for most of this period. Because free response is composed only of the natural modes of the system, it was not clear *a priori* that wave phenomenon at non-resonant frequencies would be observed. Furthermore, a mathematical formulation did not exist for expecting that the Fourier transform of the the beam's response would be composed of only a sum of waves at any frequency. This formulation is presented here and indicates that if the structure has zero initial conditions and the Fourier transform is taken over a sufficiently large time window, such that the response has decayed, then the responses at any transform frequency may be represented as a sum of waves. Furthermore, the numerical and experimental results support the hypothesis that damping can be estimated over a broad frequency range using an excitation of short duration.

This work was motivated by the need to assess damping in shock-loaded truss structures composed of many box beams filled with small viscoelastic beads. Phillips [4] recently presented experimental results of such a truss and found that the beads substantially increased the damping of the truss. One way of investigating the vibrational characteristics of many truss designs, as well as their interactions with attached structures, without fabricating them is to construct and interrogate finite element models. However, the loss factor associated with each beam is difficult to estimate, as it depends on the details, such as bead sizes and their dynamic interactions. This difficulty is overcome by performing experiments on one section of a beam and using the experimental data to estimate the loss factor in the band of interest. Because the loss factor of a filled beam is known to be a strong function of frequency, as experimentally demonstrated by House [5], we desire loss factor estimates at many frequencies in the band. These estimates are made possible by the method described here.

Section 2 presents the theoretical foundation for the method. Expressions for wave and modal estimates of the loss factor are derived. The transient response is expressed as a sum of a wave solution and a modal solution. Because the initial conditions are zero for a shock event, the modal solution is identically zero and the Fourier transform of the transient response may, at each frequency, be written as a sum of four damped waves. Once the forcing has ended, however, a transient modal solution can be obtained. In section 3, the wave model is applied to a finite element beam model as well as actual beam data. Using the finite element model, the frequency bounds of the loss factor estimation procedure are investigated. The

results are then applied to the analysis of bead-filled box beam and a comparison is made to modal damping estimates. The paper concludes with guidelines for use of the method.

2. DAMPING THEORY

In developing the solution for the forced response, the premise of this paper is that the total solution, $y(x, t)$, can be written as a sum of wave and modal solutions:

$$y(x, t) = y_w(x, t) + y_m(x, t). \tag{1}$$

Here, y_w represents the wave solution which is required to satisfy homogeneous initial conditions and non-homogeneous boundary conditions. The modal solution, y_m , is required to satisfy non-homogeneous initial conditions and homogeneous boundary conditions. In other words, the modal solution accounts for non-zero initial conditions, $y(x, t = 0)$ and the wave solution accounts for forcing terms appearing in the boundary conditions.

The differential equation which both the modal and wave solutions must satisfy is given by

$$\rho \, d^2y/dt^2 + \mathcal{L}\{y\} = 0, \tag{2}$$

where \mathcal{L} is a time-invariant linear operator involving derivatives with respect to x . It is subject to boundary conditions of the form

$$\mathcal{L}_b\{y\} |_{x=x_b} = \begin{cases} f(t), & \text{wave solution,} \\ 0, & \text{modal solution,} \end{cases} \tag{3}$$

in which $x_b = \{0, L\}$ and \mathcal{L}_b is time-invariant and involves spatial derivatives of y . The boundary forcing is such that $f(t < 0) = 0$ and $\lim_{t \rightarrow \infty} f(t) = 0$.

The modal response to non-zero initial conditions is the approach commonly employed in modelling transient response data. Only the wave solution due to transient forcing will be developed here. In particular, the equations will be presented in the context of a free-free beam excited by a shear force at one end.

2.1. WAVE SOLUTION

The form of equation (2) describing a free-free beam is

$$m \frac{\partial^2 y_w}{\partial t^2} + EI \frac{\partial^4 y_w}{\partial x^4} = 0. \tag{4}$$

Homogeneous initial conditions are assumed:

$$y_w(x, t = 0) = 0, \quad \dot{y}_w(x, t = 0) = 0 \tag{5, 6}$$

The boundary conditions of equation (3) are given by

$$\begin{aligned}
 M(x = 0, t) = EI \frac{\partial^2 y_w}{\partial x^2} \Big|_{x=0} = 0, \quad Q(x = 0, t) = -EI \frac{\partial^3 y_w}{\partial x^3} \Big|_{x=0} = f(t), \\
 M(x = L, t) = EI \frac{\partial^2 y_w}{\partial x^2} \Big|_{x=L} = 0, \quad Q(x = L, t) = -EI \frac{\partial^3 y_w}{\partial x^3} \Big|_{x=L} = 0.
 \end{aligned} \tag{7}$$

Equations (4) and (7) will be transformed with respect to time using the Fourier transform pair

$$G(\omega) = \frac{1}{2\pi} \int_{-\infty}^{\infty} g(t)e^{i\omega t} dt, \quad g(t) = \int_{-\infty}^{\infty} G(\omega)e^{-i\omega t} d\omega. \tag{8}$$

Employing the homogeneous initial conditions (5) and assuming that $\lim_{t \rightarrow \infty} y_w(t) = 0$, the transformed beam equation (4) is given by

$$E(1 - i\eta(\omega))I \frac{\partial^4 Y_w(x, \omega)}{\partial x^4} - \omega^2 m Y_w(x, \omega) = 0, \tag{9}$$

where damping has been introduced in the frequency domain through a complex modulus of elasticity, $E(1 - i\eta(\omega))$.

The solution of this homogeneous equation is of the form

$$Y_w(x, \omega) = c_1(\omega)e^{ikx} + c_2(\omega)e^{-ikx} + c_3(\omega)e^{kx} + c_4(\omega)e^{-kx}, \tag{10}$$

where

$$k = {}^{1/4}\sqrt{\frac{\omega^2 m}{E(1 - i\eta(\omega))I}} \tag{11}$$

is complex due to damping. The first two terms correspond to flexural waves propagating from each end of the beam. The latter two terms correspond to evanescent waves decaying from each end of the beam. Damping causes the flexural waves to decay, and the evanescent waves to oscillate, along the length of the beam.

The complex constants $c_1(\omega)$ through $c_4(\omega)$ are obtained by forcing equation (10) to satisfy the transformed non-homogeneous boundary conditions (7). The following set of simultaneous algebraic equations results when the complex modulus is inserted in the transformed boundary conditions:

$$\begin{bmatrix} (ik)^2 & (-ik)^2 & (k)^2 & (-k)^2 \\ (ik)^3 & (-ik)^3 & (k)^3 & (-k)^3 \\ (ik)^2 e^{ikL} & (-ik)^2 e^{-ikL} & (k)^2 e^{kL} & (-k)^2 e^{-kL} \\ (ik)^2 e^{ikL} & (-ik)^3 e^{-ikL} & (k)^3 e^{kL} & (-k)^3 e^{-kL} \end{bmatrix} \begin{bmatrix} c_1 \\ c_2 \\ c_3 \\ c_4 \end{bmatrix} = \begin{bmatrix} 0 \\ -F(\omega) \\ 0 \\ 0 \end{bmatrix} \frac{1}{E(1 - i\eta(\omega))I}. \tag{12}$$

When the right-hand side and k are known, this equation can be solved at each frequency for the wave magnitudes $c_1(\omega)$ through $c_4(\omega)$. To obtain a non-trivial solution to equation (12), a non-zero right-hand side is the only requirement. Thus, the wave formulation presented can be applied to systems with arbitrary, albeit non-zero, boundary conditions.

The inverse transform yields the time domain solution as

$$y_w(x, t) = \int_{-\infty}^{\infty} (c_1 e^{ikx} + c_2 e^{-ikx} + c_3 e^{kx} + c_4 e^{-kx}) e^{-i\omega t} d\omega. \tag{13}$$

2.1.1. *Experimental estimation of damping*

Given zero initial conditions and forcing only at the boundaries, damping can be estimated using equation (10) when the spatial response is known at n discrete locations, $x_i, i = 1, \dots, n$ along the beam. In this case, a system of n non-linear complex algebraic equations can be written at each frequency ω :

$$\begin{bmatrix} Y_w(x_1, \omega) \\ Y_w(x_2, \omega) \\ \vdots \\ Y_w(x_n, \omega) \end{bmatrix} = \begin{bmatrix} e^{ikx_1}, & e^{-ikx_1}, & e^{kx_1}, & e^{-kx_1}, \\ e^{ikx_2}, & e^{-ikx_2}, & e^{kx_2}, & e^{-ikx_2}, \\ \vdots & \vdots & \vdots & \vdots \\ e^{ikx_n}, & e^{-ikx_n}, & e^{kx_n}, & e^{-kx_n}, \end{bmatrix} \begin{bmatrix} c_1(\omega) \\ c_2(\omega) \\ c_3(\omega) \\ c_4(\omega) \end{bmatrix}. \tag{14}$$

Given a guess of $k(\omega) = k_R(\omega) + ik_I(\omega)$, the wave magnitudes c_1, \dots, c_4 can be estimated using linear least squares. Thus, any non-linear optimization algorithm can be employed to find the $k(\omega)$ which minimizes an error function computed with this least-squares solution. The error function used in the examples of the next section is the normalized mean square error, ε , defined by

$$\varepsilon = \sqrt{\left(\sum_{i=1}^n |Y_e(x_i, \omega) - Y_a(x_i, \omega)|^2 \right) / \left(\sum_{i=1}^n |Y_a(x_i, \omega)|^2 \right)}. \tag{15}$$

where $Y_e(x_i, \omega)$ and $Y_a(x_i, \omega)$ are the estimated and actual wavefields respectively. Given the error minimizing $k_e(\omega)$, the estimated loss factor is given by

$$\eta_e(\omega) = \left| \frac{\Im\{k_e^4\}}{\Re\{k_e^4\}} \right|, \quad \omega > 0. \tag{16}$$

2.2. MODAL SOLUTION

A modal solution exists which satisfies equation (4), but with non-homogeneous initial conditions

$$y_m(x, t = 0) = y_0(x), \quad \dot{y}_m(x, t = 0) = \dot{y}_0(x) \tag{17, 18}$$

and homogeneous boundary conditions given by

$$\begin{aligned}
 M(x = 0, t) = EI \frac{\partial^2 y_w}{\partial x^2} \Big|_{x=0} &= 0, & Q(x = 0, t) = -EI \frac{\partial^3 y_w}{\partial x^3} \Big|_{x=0} &= 0, \\
 M(x = L, t) = EI \frac{\partial^2 y_w}{\partial x^2} \Big|_{x=L} &= 0, & Q(x = L, t) = -EI \frac{\partial^3 y_w}{\partial x^3} \Big|_{x=L} &= 0.
 \end{aligned} \tag{19}$$

The modal solution takes the form

$$y_m(x, t) = \sum_{j=1}^{\infty} \Phi_j(x) \gamma_j(t), \tag{20}$$

where $\Phi_j(x)$ and $\gamma_j(t)$ must satisfy

$$\frac{\partial \Phi_j}{\partial x} + k_j^4 \Phi_j(x) = 0, \tag{21}$$

$$\ddot{\gamma}_j(t) + (1 - i\eta_j)\omega_j^2 \gamma_j(t) = 0 \tag{22}$$

and

$$k_j^4 = \rho A \omega_j^2 / EI. \tag{23}$$

Recall that in the wave model, the entire complex modulus, $E(1 - i\eta)$, appears in the spatial equation (9). Here, it is factored such that the real modulus E appears in the spatial equation (21) and the complex damping factor in the temporal equation (22).

The temporal solution for the j th mode takes the form

$$\gamma_j(t) = A_j e^{-i\omega_j \sqrt{1 - i\eta_j} t} + A_j^* e^{i\omega_j \sqrt{1 - i\eta_j} t}, \tag{24}$$

where the positive value of ω_j is assumed and η is an odd function evaluated at $\eta_j = \eta(\omega_j > 0)$. A and A^* are complex conjugates that are related to the modal initial conditions by

$$\Re\{A_j\} = \gamma_j(0)/2, \tag{25}$$

$$\Im\{A_j\} = \frac{\dot{\gamma}_j(0) - \gamma_j(0)\omega_j \Im\{\sqrt{1 - i\eta_j}\}}{2\omega_j \Re\{\sqrt{1 - i\eta_j}\}}. \tag{26}$$

Numerical techniques can be employed to fit the modal solution of equations (20) and (24) to transient response data. The damping factor, η , can be obtained

from the complex frequencies of equation (24), $\omega_{cj} = \omega_j \sqrt{1 \pm i\eta_j}$, as

$$\eta_j = \left| \frac{\Im\{\omega_{cj}^2\}}{\Re\{\omega_{cj}^2\}} \right|. \tag{27}$$

3. EXAMPLES

The proposed approach to modelling loss factor was tested on simulated as well as experimental data. In the simulation, a transient shear load was applied to one end of a finite element beam model. The goal of the simulation was to compare damping estimates obtained using modal and wave techniques for a system with a prescribed level of damping. The damping consisted of stiffness-dependent Rayleigh damping. The remaining model properties and loading were selected to match a beam experiment which is also described here. In the experiment, a box beam was filled with granular material to enhance damping. The beam was struck transversely at one end with an instrumented sledge hammer. In this case, the actual damping is unknown. Prior experiments in which sinusoidal excitation was applied suggest that damping is strongly dependent on frequency. Simulation and experimental results are both described below.

3.1. FINITE ELEMENT BEAM MODEL

The model was composed of 12 Euler–Bernoulli cubic beam elements with the properties listed in Table 1. The moment of inertia was computed based on the cross-section of the empty box beam. The mass per unit length corresponded to that of the box beam when filled with granular material. The prescribed Rayleigh damping was of the form

$$[C] = \alpha[M] + \beta[K] \tag{28}$$

with $\alpha = 0$ and so

$$\eta(\omega) = \omega\beta. \tag{29}$$

TABLE 1
Properties of finite element beam model

Property	Value
E , elastic modulus	30×10^6 psi
I , moment of inertia	68.7 in ⁴
L , length	16 ft
m , mass per unit length	0.129 slugs/ft
α	0
β	2×10^{-4}

An actual hammer blow, sampled at 5 kHz, was applied as a shear force at $x = 0$. Measurements of transverse acceleration $a(x, t)$ were assumed available at 13 points positioned 16 in apart along the beam.

To verify the presence of waves in the data, a frequency-wavenumber transform can be employed by computing a two-dimensional Fourier transform of the acceleration data, $a(x, t)$,

$$\mathcal{A}(\omega, k) = \frac{1}{(2\pi)^2} \int_0^T \int_0^L a(x, t) e^{i(kx + \omega t)} dx dt. \tag{30}$$

The transform $\mathcal{A}(\omega, k)$ is maximized whenever the wavenumber and frequency (k, ω) coincide with that of a natural wave, (k_n, ω_n) , as described by

$$a(x, t) = \Re \{ A e^{i(k_n x - \omega_n t)} \}. \tag{31}$$

Note that equation (31) represents a forward going wave and so $\mathcal{A}(\omega, k)$ will be maximized for $k = -k_n < 0$.

Figure 1 depicts the frequency-wavenumber transform for a typical high-amplitude hammer hit. Rearranging equation (11), we obtain

$$\omega \approx \sqrt{\frac{EI}{m}} k^2, \quad \omega\beta \ll 1. \tag{32}$$

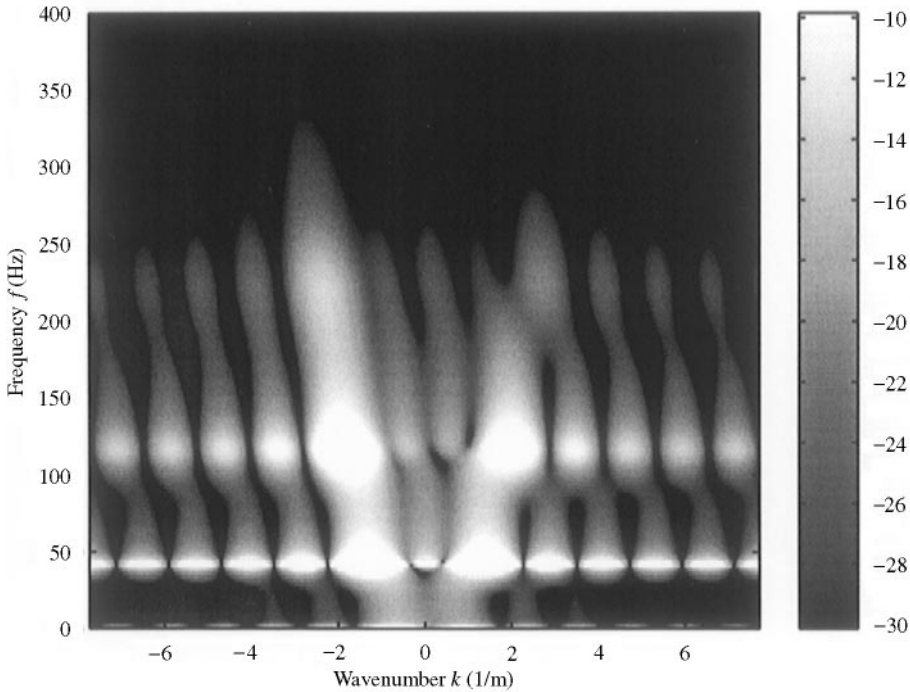


Figure 1. Frequency-wavenumber transform of finite element model acceleration response.

The two branches of this parabola are clearly visible in Figure 1 for $0 \leq \omega \leq 300$ Hz. The coarse spacing of the 13 accelerometers produces side lobes to the left and right of this parabola. They are particularly strong at the modal frequencies of the beam, i.e., $f = 42, 118, 228$ Hz. Note that the left branch of the parabola ($k < 0$) corresponds to the wave leaving the impacted end of the beam. The right branch ($k > 0$) corresponds to the wave reflected from the far end. Owing to damping, it can be seen that the magnitude of the reflected wave is reduced.

3.1.1. Loss factor estimation

The loss factor was estimated using equations (14)–(16) and the 13 numerically computed accelerations. To gain insight into the sensitivity of the estimation procedure, normally distributed noise with a variance of 0.98 m/s^2 (white with respect to time) was added to the acceleration data. The exact and estimated damping factors are depicted in Figure 2. Note that no attempt was made to estimate spatial damping at frequencies for which the beam length is less than half a wavelength. This is due to the weak dependence of the implemented error function on damping when evaluated over fractions of a wavelength. Thus, the abscissa starts at the first modal frequency.

Following equation (29), the exact stiffness-proportional Rayleigh damping is linear in frequency. The noise-free solution closely follows the exact solution, except for several fluctuations above 300 Hz. Similarly, agreement between the exact and noisy-data estimate is good below 300 Hz. Above 300 Hz, the estimated loss factor fluctuates widely with frequency, but with an average value approximating the

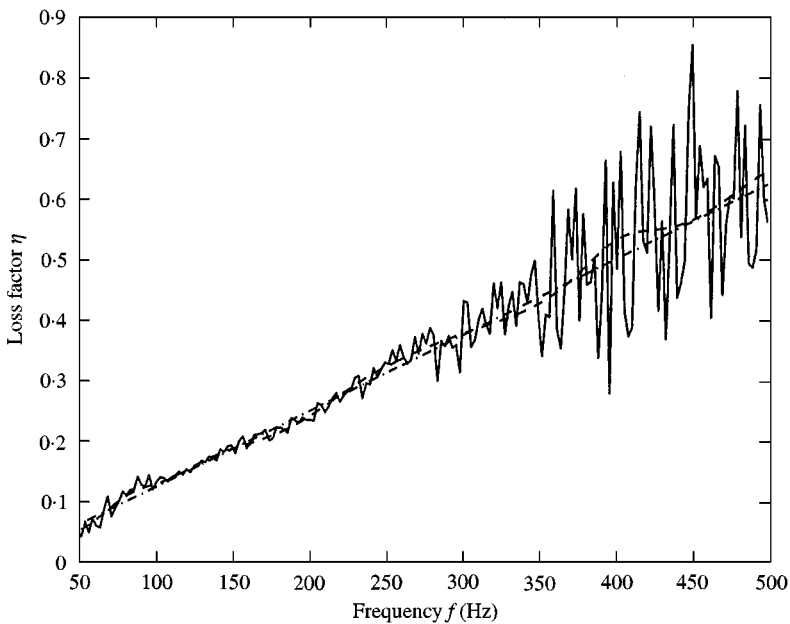


Figure 2. Loss factor versus frequency for the finite element model: - - -, exact solution; - · -, estimate from noise-free simulated data; —, estimate from noisy simulated data.

exact solution. Returning to Figure 1, this result is not surprising, as it is clear that the wave energy falls off between 250 and 300 Hz.

With experimental data, the exact loss factor and signal noise are unknown. Consequently, it is worthwhile to investigate measures by which an upper frequency bound can be ascertained. A natural choice is to use the error function, ε , employed in the estimation procedure. Normalized mean square error, given by equation (15), is plotted in Figure 3. This figure confirms the observations regarding loss factor. For the noisy case, the error rapidly increases above 250 Hz. While of much smaller magnitude, the noise-free error also increases rapidly above 250 Hz.

From Figure 1, it is clear that loss factor estimation using a wave model is only appropriate for frequencies at which a wave of sufficient magnitude is present in the data. Thus, the upper frequency bound for noise-free estimation is determined by the energy distribution of the impact as well as by the loss factor itself. As described in the paragraph below, the major effect of additive acceleration noise is to reduce this upper frequency bound.

Figures 1–3 clearly show that the addition of noise has a modest effect on loss factor estimation for high amplitude waves (and consequently high acceleration measurements). As frequency increases, however, wave amplitude falls off and (assuming frequency-independent noise amplitude) the noise begins to obscure the magnitude and phase relationship between the acceleration measurements along the beam. This can be seen in Figure 4 which depicts the magnitudes of the 13 acceleration measurements used in the example. Recall from equation (14) that the estimation procedure involves fitting a sum of four waves to these measurements at

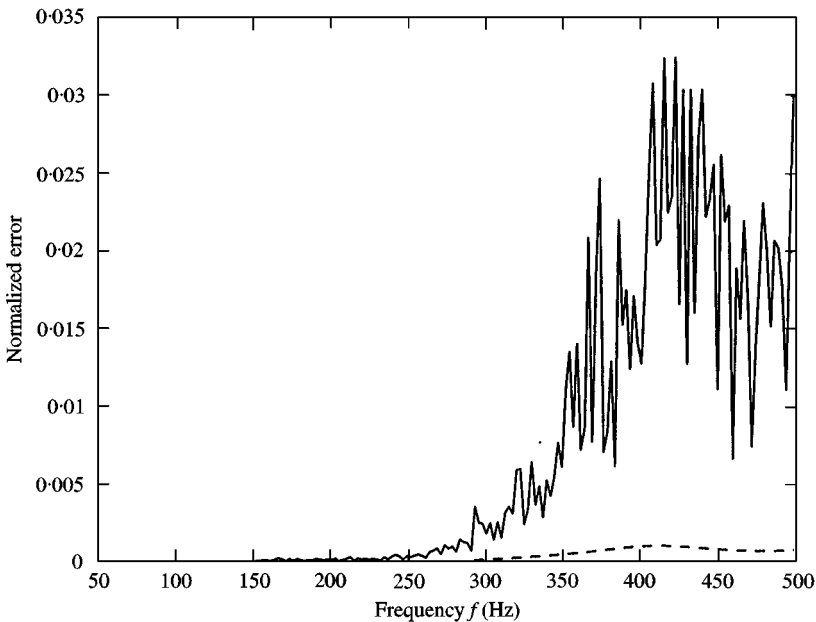


Figure 3. Normalized mean square error versus frequency for the simulated data: ---, without noise; —, with noise.

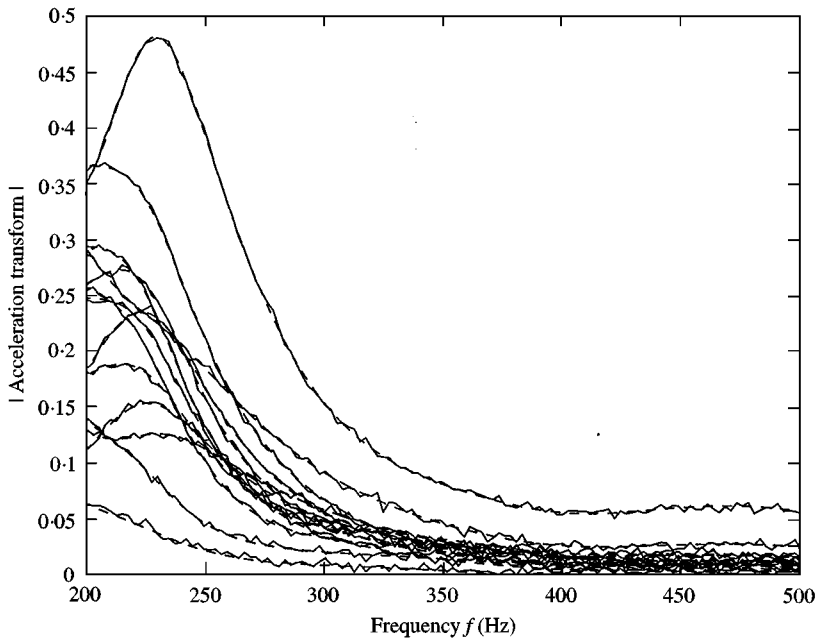


Figure 4. Magnitude of transformed acceleration versus frequency for the 13 accelerometers: ---, without noise; —, with noise. Note that noise dominates relative magnitudes above 250 Hz.

each frequency. From 200 to 250 Hz, the magnitude relationship of the signals is unaffected by the noise. Above 250 Hz, however, the noise dominates the relative acceleration magnitude for many acceleration pairs.

3.2. FILLED BOX BEAM

A steel box beam with cross-section $10'' \times 6'' \times 3/8''$ and length 16' was suspended horizontally by elastic cords to approximate free-free boundary conditions. The beam configuration is depicted in Figure 5 and the cross section is shown in Figure 6. The elastic cords were $3/4''$ in diameter and 20 ft in length. Steel plate endcap assemblies, with dimensions of approximately $12'' \times 8'' \times 3/4''$, were bolted to both ends of the beam for convenient installation of the fill materials. The two end plates have equal weight. With a total beam weight of approximately 603 lb, the frequencies due to the suspension are estimated at less than 5 Hz.

Chevron LDPE 1117B beads were used as the granular fill material. This material is widely used in injection molding. The weight density of the packed LDPE beads was 36.8 lb/ft^3 . The volume available to the fill material was 5.40 ft^3 . During the filling process, vibrations were applied to the beam (by tapping with a hammer) to ensure the granular material was well packed in the beam.

As shown in Figure 5, 13 accelerometers were placed 16 in apart on the beam along the horizontal plane passing through the center of the cross section. The number and spacing of accelerometers was chosen so as to provide approximately

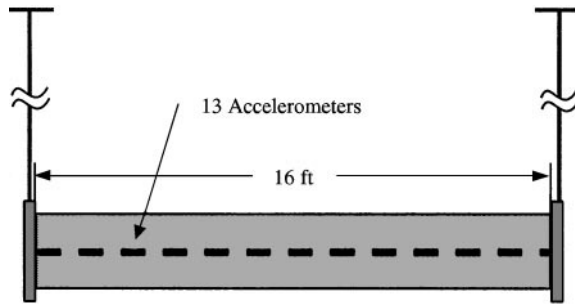


Figure 5. Beam schematic.

6 points per wave for the 4th bending mode. The uniaxial accelerometers used in the test were calibrated to 50 g's.

3.2.1. Experimental procedure

Flexural vibrations were excited in the horizontal plane as depicted in Figures 5 and 6. The impact forces were generated by a transverse hammer blow to one end plate on the side opposite the accelerometers. The accelerations and impact force were recorded at a sampling rate of 5 kHz using a 1 kHz low-pass filter.

Ten trials of varying impact amplitude were conducted for the filled beam. The four with the highest impact amplitudes were deemed to possess a sufficient signal to noise ratio up to 300 Hz to employ a wave model for loss factor estimation. For a typical trial, Figure 7 depicts the time histories of the accelerometers at the beam's impact end ($x = 0$) and far end ($x = l$). The wave speed can be deduced from the time it takes for the first peak to reach the far end of the beam. A comparison of the amplitudes of the accelerometers' first peaks demonstrates the existence of spatial damping. For $t > 0.3$ s, the modal character of the data is apparent with the response dominated by frequencies of 37 and 108 Hz.

The Fourier transform of these acceleration histories is plotted in Figure 8. Five beam modes can be seen. The first two correspond to those observed in the time histories. A pendulum mode, due to the suspension, can also be observed at approximately 5 Hz. To verify the presence of waves in the experimental data, the frequency-wavenumber transform of equation (30) was employed. The result for one trial is shown in Figure 9. This figure compares favorably with the finite element model results of Figure 1.

It should be noted that box beams—empty and filled—are capable of producing plate waves which travel along the sides of the beam. Both analytical predictions and frequency wavenumber transforms of the data indicate that these waves cut on at approximately 500 Hz. Consequently, they will not be considered here.

3.2.2. Loss factor estimation

Equations (14)–(16) were used to obtain a wave model estimate of the loss factor. As this model requires non-zero boundary conditions and zero initial conditions, the first 15 000 data points (3 s duration) were used for loss factor estimation. For

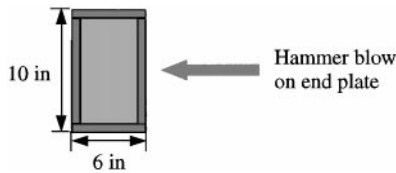


Figure 6. Beam cross-section: ■, 3/8 in steel; □, granular material.

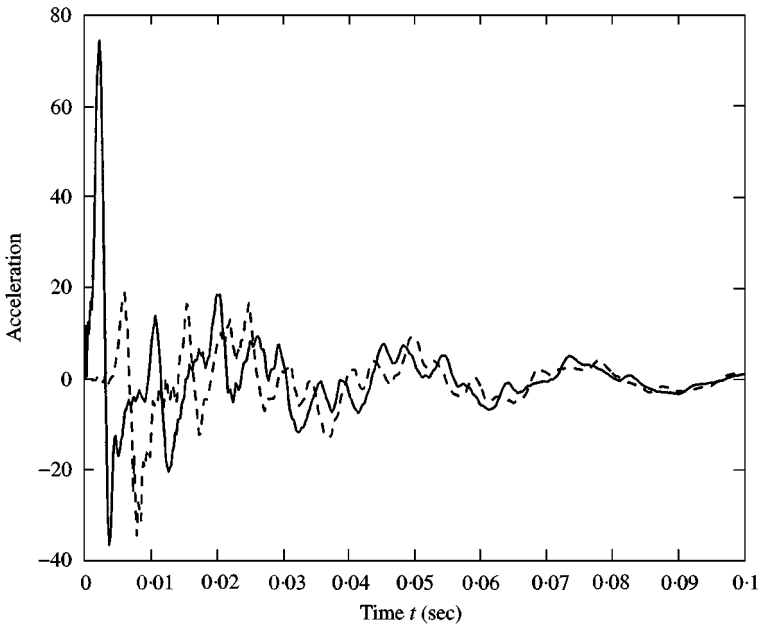


Figure 7. Acceleration (in g 's) versus time at both ends of beam: —, $x = 0$; ---, $x = L$. Shock input was at $x = 0$.

a clear depiction of the variation in loss factor estimates between the four trials considered, the maximum and minimum envelope curves are plotted in Figure 10. Similarly, the maximum and minimum normalized error is plotted in Figure 11. Note that the knee of the error curve occurs at about 225 Hz. Based on the FEM results (recall Figure 3), the wave damping estimates are valid up to this frequency.

As a result, these estimates can be compared to modal estimates obtained using equations (20), (24) and (27) at the first three modal frequencies of 37, 108 and 207 Hz. Since the modal equations apply for homogeneous boundary conditions and non-zero initial conditions, a time window was employed which started after the hammer impact ended. This time corresponds to the first zero crossing of the accelerometer located at $x = 0$. Figure 7 shows this occurs at $t \approx 4$ ms. Data from the 13 accelerometers was used simultaneously in the modal damping estimate. The average modal damping factors are shown in Figure 10. The variation between trials, while not shown, was less than 0.02 for the three modes.

In Figure 10, the wave and modal loss factors are seen to be consistent at the three modal frequencies. The average wave model estimate exceeds the average

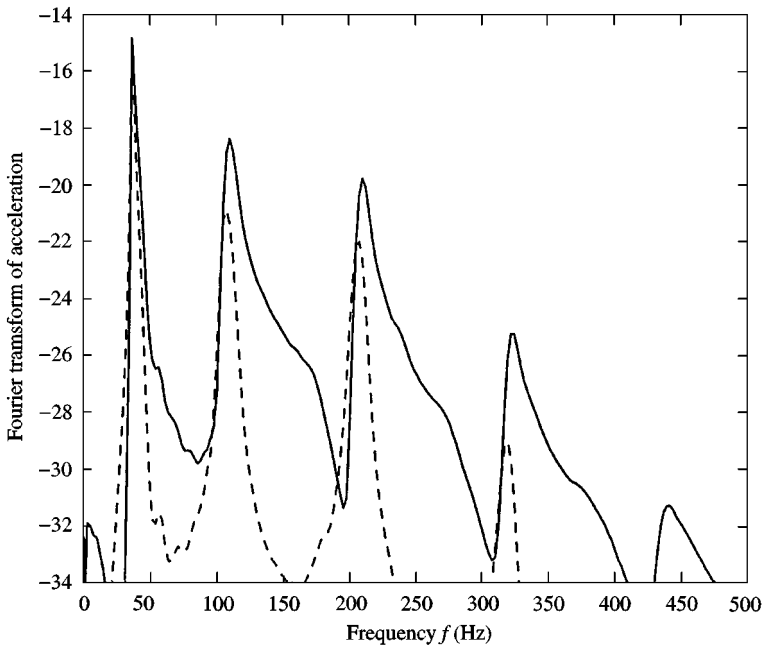


Figure 8. Acceleration versus frequency at both ends of beam: —, $x = 0$; ---, $x = L$. Shock input was at $x = 0$. Five highest peaks correspond to beam modes. 5 Hz peak is suspension frequency.

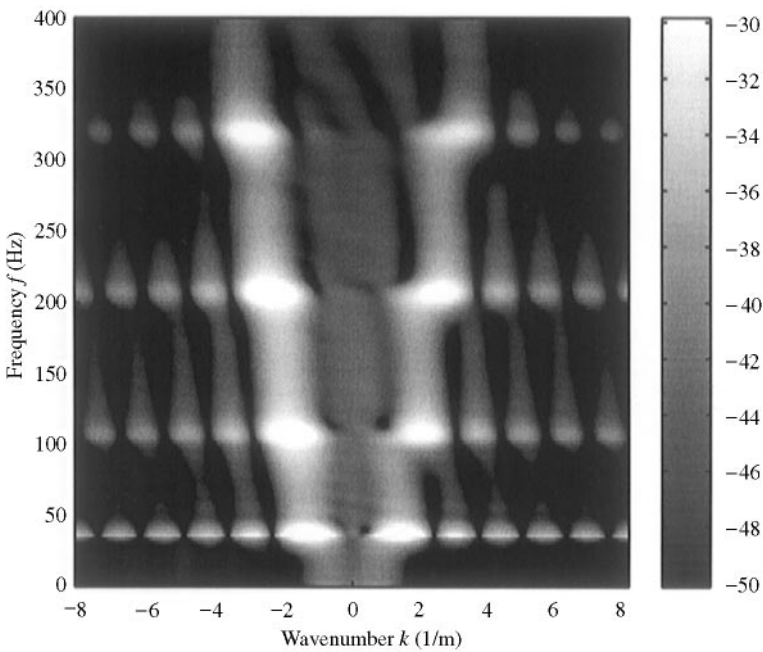


Figure 9. Frequency wavenumber transform of beam acceleration data.

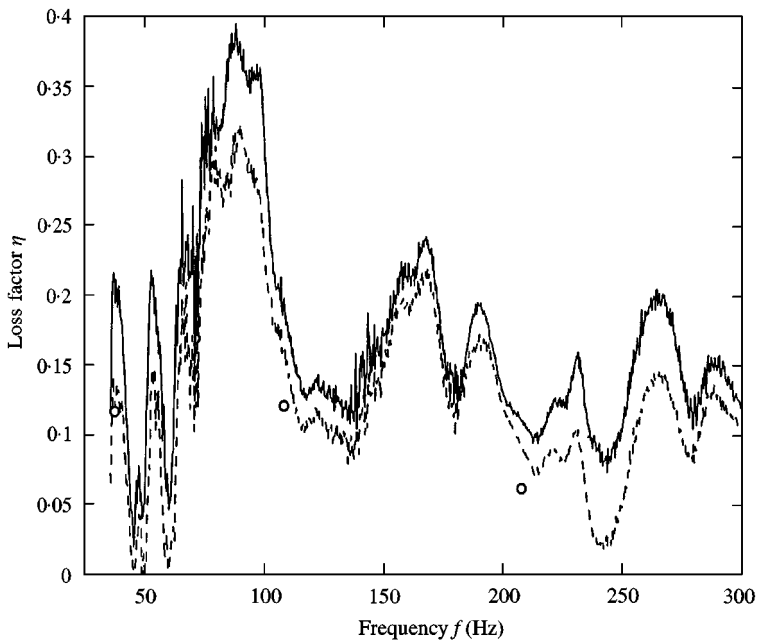


Figure 10. Loss factor versus frequency for four trials: —, wave envelope maximum; ---, wave envelope minimum; O, modal average.

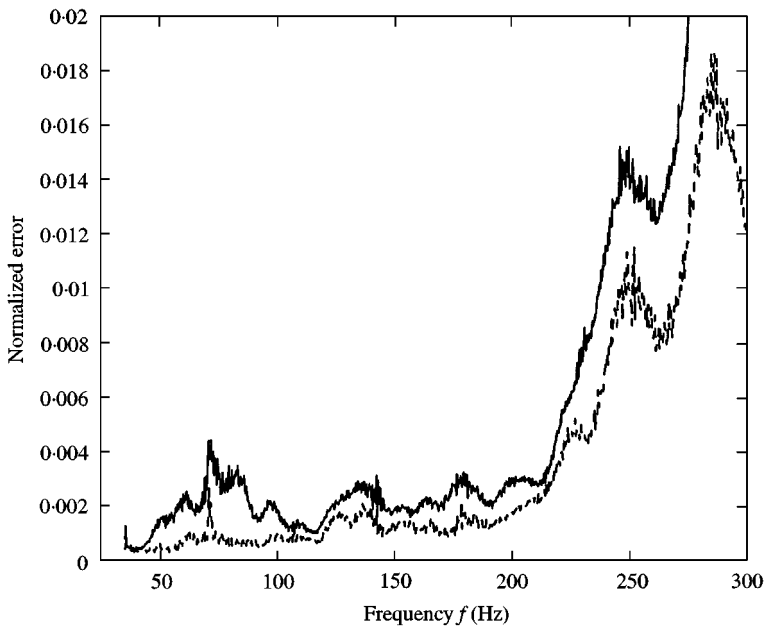


Figure 11. Normalized mean square error versus frequency for four trials: —, envelope maximum; ---, envelope minimum.

modal estimate by 0.05 for the first two modes and 0.03 for the third mode. In addition, greater variation between trials was observed with the wave method.

It is likely that the higher damping estimate obtained by the wave method can be attributed to the difference in data records used with the two methods. Recall that the wave data record must include the time duration of the hammer impact while the modal data record must exclude these data. Thus the modal data window excludes $t \leq 4$ ms shown in Figure 7. While short in comparison to the total temporal record length, note that the omitted acceleration peak at $x = 0$ is five times the value of the first included peak.

It is probable that damping is higher during this initial, high-amplitude time period. This may be due to nonlinear behavior associated with beam bending. Alternatively, starting from rest, the rate of energy absorption by the granular fill may initially exceed its rate of dissipation. From the perspective of the beam's motion, damping would initially be high and decrease until the granular fill reached "steady state" motion in response to forcing by the beam. The inclusion of this early-time data would increase the average damping observed over the time window.

The greater trial-to-trial variation in wave-based loss factor estimation is due to the use of a spatial discretization (13 locations) which is coarse in comparison to the temporal discretization employed in the modal estimate. At the third modal frequency (207 Hz), this corresponds to 4 spatial points per wavelength compared to 20 temporal points per wavelength. A larger number of points per wavelength reduces the effect of sensor noise on the estimate.

4. CONCLUSIONS

The wave method complements traditional modal techniques by making it possible to estimate the loss factor at regularly spaced frequency values—not just at modal frequencies. The method is applicable for arbitrary forcing applied through the boundary conditions. Furthermore, no specific knowledge of the structure's boundary conditions, material properties or cross-sectional dimensions is required. Since the measurements are Fourier transformed, the data record must be of sufficient duration for the transform to converge. Except when damping depends strongly on amplitude or time, however, this condition is easily met.

The frequency range over which damping can be estimated is limited by several factors. Given a fixed amount of energy at a frequency, the actual loss factor must be large enough to separate wave decay along the length of the beam from signal noise. Thus, there must be sufficient wave energy due to the boundary forcing to produce an acceptable signal to noise ratio. Since realistic forcing is band limited, this condition imposes an upper bound on estimation frequency. Normalized estimation error was found to provide a practical means of determining this upper bound. In addition, when the ratio of wavelength to beam length (λ/L) is large, normalized error is a weak function of loss factor. This imposes a lower bound on estimation frequency. Analysis of numerically and experimentally generated beam data indicates that the first modal frequency ($\lambda/L = 2$) is an adequate lower bound.

ACKNOWLEDGMENT

This work was supported by the Office of Naval Research under grant no. N00014-98-1-0755.

REFERENCES

1. T. PLONA, B. SINHA, S. KOSTEK and S. CHANG 1992 *The Journal of the Acoustical Society of America* **92**, 1144–1155. Axisymmetric wave propagation in fluid-loaded cylindrical shells. II: theory versus experiment.
2. J. VOLLMANN, R. BREU and J. DUAL 1997 *The Journal of the Acoustical Society of America* **102**, 909–920. High-resolution analysis of the complex wave spectrum in a cylindrical shell containing a viscoelastic medium. 2. Experimental results versus theory.
3. J. MCDANIEL, K. LEPAGE and N. MARTIN 1995 *The Journal of the Acoustical Society of America* **98**, 2889. Computation of complex wavenumbers and amplitudes of vibrating structures.
4. J. PHILLIPS 1996 *Proceedings of the 16th Aerospace Testing Seminar*, 355–365. Vibration testing of titan IV-A instrumentation truss with polymeric bead damping.
5. J. HOUSE 1989 *Polymeric Materials: Science and Engineering, Proceedings of the ACS Division* **60**, 734–738. Damping hollow tubular structures with lightweight visco-elastic spheres.